JOURNAL OF APPLIED CRYSTALLOGRAPHY

ISSN 1600-5767

Received 25 February 2019
Accepted 25 July 2019

Edited by A. Borbély, Ecole National Supérieure des Mines, Saint-Etienne, France

Keywords: X-ray micro-diffraction; differential aperture X-ray microscopy; DAXM; *in situ* deformation; sample alignment; digital image correlation; DIC.

Alignment of sample position and rotation during *in situ* synchrotron X-ray micro-diffraction experiments using a Laue cross-correlation approach

Chenglu Zhang,[a] Yubin Zhang,[b] Guilin Wu,[c] Wenjun Liu,[d] Ruqing Xu,[d] Dorte Juul Jensen[b] and Andrew Godfrey[a]*

[a]Key Laboratory of Advanced Materials (MOE), School of Materials Science and Engineering, Tsinghua University, Beijing, 100084, People's Republic of China, [b]Department of Mechanical Engineering, Technical University of Denmark, Kongens Lyngby, 2800, Denmark, [c]College of Materials Science and Engineering, Chongqing University, Chongqing, 400045, People's Republic of China, and [d]Advanced Photon Source, Argonne National Laboratory, Argonne, Illinois 60439, USA. *Correspondence e-mail: awgodfrey@mail.tsinghua.edu.cn

Laue micro-diffraction has proven to be able to reveal material properties at the sub-grain scale for many polycrystalline materials and is now routinely available at several synchrotron facilities, providing an approach for nondestructive three-dimensional probing of the microstructures and mechanical states of materials. However, for *in situ* experiments, maintaining the positioning of the sample throughout the experiment, to achieve a good alignment of the characterized volumes, is a challenging issue. The aim of the present work is to address this problem by developing an approach based on digital image correlation of focused-beam Laue diffraction patterns. The method uses small changes in the diffraction signal as a focused X-ray beam is scanned over a surface region to allow corrections to be made for both sample lateral movement and rotation. The method is demonstrated using a tensile deformation experiment on an Al sample with 2.5 µm average grain size. The results demonstrate an accuracy of 0.5 µm for sample position registration and a precision in sample rotation of $\sim$0.01°. The proposed method is fast to implement and does not require the use of additional surface markers.

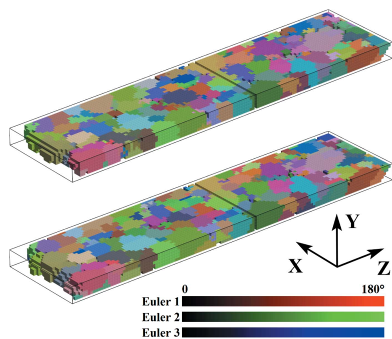

© 2019 International Union of Crystallography

1. Introduction

Over the past 20 years, a variety of novel 3D characterization techniques based on synchrotron X-rays have undergone rapid development, providing powerful tools for nondestructive investigations of the microstructures and stress/strain states of crystalline materials. These techniques, including 3D X-ray diffraction (Poulsen, 2004, 2012), X-ray diffraction contrast tomography (Ludwig *et al.*, 2008; Johnson *et al.*, 2008), dark-field X-ray microscopy (Simons *et al.*, 2015; Ahl *et al.*, 2017) and differential aperture X-ray microscopy (DAXM) (Larson *et al.*, 2002; Larson & Levine, 2013), are all diffraction based. The former three utilize monochromatic parallel X-rays and tomographic data-acquisition methods, while the latter utilizes polychromatic focused X-rays, with use of a differential aperture for depth resolution of Laue diffraction patterns collected in a scanning mode. By coupling 3D characterization with external thermal or mechanical loading (Pantleon *et al.*, 2009; Balogh *et al.*, 2013; C. L. Zhang *et al.*, 2017; M. Zhang *et al.*, 2017), unprecedented 4D (x, y, z, t) data sets, revealing microstructural evolution at critical mesoscopic length scales, can be obtained.

An important issue for performing such *in*/*ex situ* experiments is maintaining the alignment of the sample position, as any sample movement relative to the incident X-ray beam due to *in situ* loading (mechanical, thermal or otherwise) or due to sample remounting will result in a mismatch between the characterized volumes. This is particularly an issue for situations where the experimental conditions only allow a relatively small volume to be investigated. For example, for high-spatial-resolution experiments on fine-grained materials, even small positional errors can lead to an overlap failure of the interrogated volumes. One approach to address this problem involves the use of identifiable fiducial markers attached to the sample surface (Shade *et al.*, 2016). Such markers, typically of Pt or Au, can be detected via either X-ray fluorescence or diffraction methods (Guo *et al.*, 2015), and therefore can be tracked throughout the experiment. However, the deposition of such markers requires the markers to be prepared in advance of the X-ray experiment with no freedom left for last minute (or on the fly) changes of plan.

In addition to sample movement during loading, there is also a possibility of introducing a rigid-body sample rotation, in particular for mechanical loading if the loading train or mounting system is not sufficiently rigid. Although such a rotation may be small, for some investigations a high orientation accuracy may be critical (Margulies *et al.*, 2001) in order to fully exploit the high angular resolution ($\sim$0.01°) of the diffraction data. An example is analysis of experimental data collected at small plastic strains (*e.g.* near yielding), where the crystallographic lattice rotations are also expected to be very small.

2. Methodology

2.1. Sample movement

In this article, we present a new method for achieving registration of experimental volumes in 3D synchrotron X-ray experiments using DAXM. The method is based on digital image correlation (DIC) (Sutton *et al.*, 2009) of Laue diffraction patterns (Petit *et al.*, 2015; F. G. Zhang *et al.*, 2017). The sample alignment method requires no pre-made extrinsic features, and both sample movement and rotation can be corrected with high efficiency and accuracy. Demonstrations based on experimental data for samples with an average grain size in the near-micrometre regime show that a positional accuracy of 0.5 µm and an angular precision of 0.01° can be achieved.

This registration method is developed for *in situ* loading experiments using DAXM, where 3D bulk crystallographic data are obtained by scanning a microbeam (focused X-ray beam) in a grid over a sample surface. The basic idea is to first obtain the Laue diffraction pattern with the microbeam at a given position on the sample (typically the centre of the scanned area of interest), and then after loading to find this same position again using DIC, by determining the location where the microbeam Laue diffraction pattern has the greatest similarity to the initially collected pattern (before loading).

A schematic of the idea behind the method is given in Fig. 1. A focused polychromatic X-ray beam illuminates a bulk sample and generates diffraction signal from the illuminated volume (nominally a cylindrical volume extending to a certain depth depending on the X-ray energy and sample composition). The diffraction signal is collected on a Perkin–Elmer flat-panel area detector mounted above the sample. During data collection the sample stage is moved with the beam position fixed, but in the following for simplicity we consider the fully analogous situation where the sample is fixed and the microbeam is scanned over the sample surface. As shown in Fig. 1, at position A all grains along the line shown in red are illuminated and give rise to diffraction signals on the detector, in this case from grains coloured either red or green. When the X-ray beam is moved from position A to B, a new volume is illuminated. If the displacement of the beam from A to B is smaller than the grain size some grains will, however, remain illuminated (the green grains in Fig. 1), whereas some grains will no longer be illuminated (red grains), and some new grains will be illuminated (blue grains). Accordingly, some diffraction spots are seen on the detector at both positions (shown by green stars), whereas some spots appear (blue triangles) or disappear (red squares) as the beam is moved from position A to position B. If an unknown sample movement is applied and many patterns are collected with the beam incident on the surface at different positions, the position where the pattern most closely matches that at position A is the closest to the original position. Throughout this paper, the coordinate systems for the beamline and detector axis systems are plotted using uppercase and lowercase letters, respectively.

The practical procedure for implementation is as follows. An initial position reference pattern is first collected. After the sample/beam shift the beam is scanned over the sample

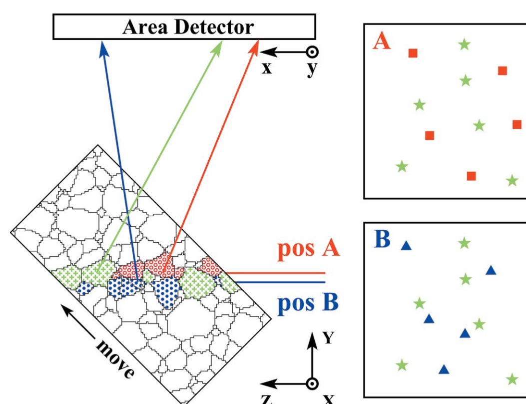

Figure 1
Schematic illustration of the basis of the Laue-CC alignment technique. With the X-ray beam incident on the sample surface at position 'A', diffraction signals are generated from a certain set of grains (here shown in red and green). If there is a movement of the sample so that the X-ray beam now is at position 'B' some change in the illuminated volume will occur – in this case the grains shown in red will no longer give rise to diffraction signals, and instead signals will be generated from the grains shown in blue. The changes in illuminated volume will result in changes in the diffraction patterns recorded in the two positions.

surface using an appropriately chosen step size and the Laue diffraction patterns collected at each position are compared using DIC with the pattern collected at the reference position. The prior position can thus be found and the sample movement corrected. The technique based on this approach is referred to hereafter as Laue cross-correlation (abbreviated to Laue-CC).

For the DIC procedure, the efficient subpixel image registration algorithm described by Guizar-Sicairos *et al.* (2008) was used. For two images $f(x, y)$ and $g(x, y)$ of the same dimensions, N by M pixels, the normalized root-mean-square error (NRMSE), E, between the images provides an error metric for good assessment of the agreement between the two images. This metric is invariant to both the global coordinate translation $(\Delta x, \Delta y)$ and multiplication by an arbitrary constant α for the image to be registered, and is defined by

$$E^2 = \min_{\alpha,\Delta x,\Delta y} \frac{\sum_{x,y} \left|\alpha g(x-\Delta x, y-\Delta y) - f(x,y)\right|^2}{\sum_{x,y} \left|f(x,y)\right|^2} = 1 - \frac{\max_{\Delta x,\Delta y} \left|r_{fg}(\Delta x, \Delta y)\right|^2}{\sum_{x,y}\left|f(x,y)\right|^2 \sum_{x,y}\left|g(x,y)\right|^2}. \quad (1)$$

Here

$$r_{fg}(\Delta x, \Delta y) = \sum_{x,y} f(x,y) g^*(x-\Delta x, y-\Delta y) = \sum_{u,v} F(u,v) G^*(u,v) \exp\left[i2\pi\left(\frac{u\Delta x}{M} + \frac{v\Delta y}{N}\right)\right] \quad (2)$$

is the cross-correlation of $f(x, y)$ and $g(x, y)$, with the asterisk (*) indicating complex conjugation and the uppercase letters F and G representing the discrete Fourier transform of their lowercase correlatives, as calculated from

$$F(u,v) = \sum_{x,y} \frac{f(x,y)}{(MN)^{1/2}} \exp\left[-i2\pi\left(\frac{ux}{M} + \frac{vy}{N}\right)\right]. \quad (3)$$

The algorithm returns the value of the NRMSE, with a lower value of this parameter corresponding to better agreement (more similarity) between the images. A simple correlation coefficient would be sufficient if image registration were the only goal of the calculation. However, as described in the next section, it is necessary also to account for global sample rotations, hence justifying the use of the equations given above.

2.2. Sample rotation

Another possible source of sample positioning error is rigid-body rotation of the sample, which will result in a shift of the spots in the diffraction pattern at a given beam position (Dingley *et al.*, 2010). In Laue diffraction with polychromatic X-rays, a sample rotation about an axis $[uvw]$ by angle θ will result in all diffraction vectors being rotated by θ about the same axis $[uvw]$. With a knowledge of the parameters describing the geometry of the detector with respect to the incident X-ray beam, the resulting displacement field representing vector shifts in the position of Laue diffraction spots on the detector for a given sample rotation can be simulated. Fig. 2(*a*) shows an example of such a simulation, corresponding to a rotation of 0.1° along the X axis in the beamline coordinate system. The geometry parameters for this simulation are taken from the experimental setup, calibrated using a strain-free silicon single crystal. The small variations in the displacement field are due to variations in the distance between each pixel on the detector and a fixed diffraction source.

In reverse, evaluation of a rigid-body sample rotation requires determination of the displacement field describing the vector shifts in diffraction spot positions between the initial and rotated condition. This information can be collected by comparing a series of regions of interest (ROIs) in two Laue patterns recorded at the same position before and after the rigid-body rotation. The vector shift representing the relative displacement of each pair of ROIs is determined using the aforementioned image registration algorithm described in equations (1)–(3) by searching for the peak in the cross-correlation function. The shift for each ROI is assigned to the position at the centre of the ROI.

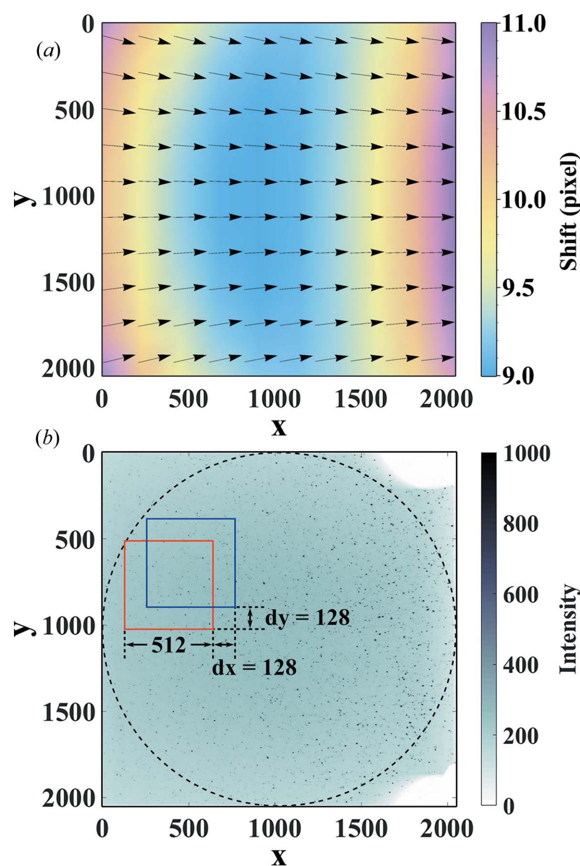

Figure 2
(*a*) Simulated displacement field for the Laue diffraction signal on the detector, assuming a sample rotation of 0.1° about the beamline X axis (see Fig. 1). The direction of the shift is shown by arrows and the magnitude of the shift by the colour scale. (*b*) Example Laue diffraction pattern (2048 × 2048 pixels) from an Al sample of 2.5 µm grain size. Two example ROIs used for sample rotation determination (512 × 512 pixels in size) are shown, offset by 128 pixels along both detector axes. The black dashed circle shows the limiting boundary for ROI placement.

Although only two ROIs are necessary to derive an estimate of the rigid-body rotation of a sample, using a larger number of ROIs permits greater accuracy by use of a least-squares fitting method. Additionally, to allow the use of a fast Fourier transform algorithm for solving equations (1)–(3), the size of each ROI should be taken as a power of 2. In our analysis, ROIs of size 512 × 512 pixels are selected with offsets of 128 pixels evenly distributed over a centred circular area of the detector, avoiding areas near the detector corners where some diffraction signal loss is present as a result of shielding from the experimental setup [see Fig. 2(*b*)]. For the data sets we have analysed to date this ROI has given good results, as a good compromise between accuracy of determining the vector shift at each ROI position and a sufficient number of ROIs to map the variation in vector shifts over the detector area. For other data sets it is recommended to determine the optimum ROI size by similar considerations. From fitting of the displacement field, the sample rotation can therefore be determined and used, for example, to calculate accurately the crystal lattice rotation at each voxel before and after applying a small deformation to the sample (see Section 3.2).

2.3. Image enhancement

In addition to Laue spots, the recorded diffraction patterns contain some noise due to detector damage (pixels with a high 'burned-in' value), as well as a smoothly varying background from X-ray fluorescence. In our experiment, the detector damage noise is characterized by a small number of isolated damaged detector pixels (typically 1 part in 100 000) with intensity at least ten times higher than the peak spot intensity. The global background noise is Gaussian in shape, covering the whole detector with a relatively low intensity. Both are independent of the local microstructure and do not vary as the beam position is moved relative to the sample. Consequently, they can be expected to lead to a deterioration of the image registration procedures described above. A common solution to this problem is the use of band-pass filtering, to attenuate both high spatial frequencies (detector noise) and low frequencies (corresponding to the Gaussian background). In our case we found it most effective to use a combination of a median filter and a high-pass filter. For the median filter, each output pixel contains the median value in a 3 × 3 neighbourhood around the corresponding pixel in the input image. In terms of high-pass filtering, for the present data set, we have found that a high-pass Butterworth filter of order 1, with a cutoff frequency of 10, has worked well for all data sets collected so far. Different parameters might be required for large changes in pattern quality/detector noise to achieve the best signal-to-noise ratio. A key point in use of this combined-filtering approach is that the high-pass filtering should always be performed after the median filtering in order to completely remove the influence of the damaged detector pixels. To evaluate the effect of various filtering approaches, a simulation was carried out with the results presented in Fig. 3. Two microbeam Laue diffraction patterns of size 2048 × 2048 pixels were recorded from the same sample (in this case a sample of recrystallized aluminium) at positions far apart, without any grain coincidence. One image was taken as a reference image. Randomly selected circular areas of radius 16 pixels in this reference image were then substituted with the same area of the second image to make a composite image. By varying the substitution fraction a series of images representing a gradual change from identical images (0% substitution) to distinctly different images (100% substitution) are simulated. Some examples are given in Fig. 3.

In each case the composite image was registered to the reference image and the NRMSE evaluated. Before registration, identical filtering was applied to both images (reference

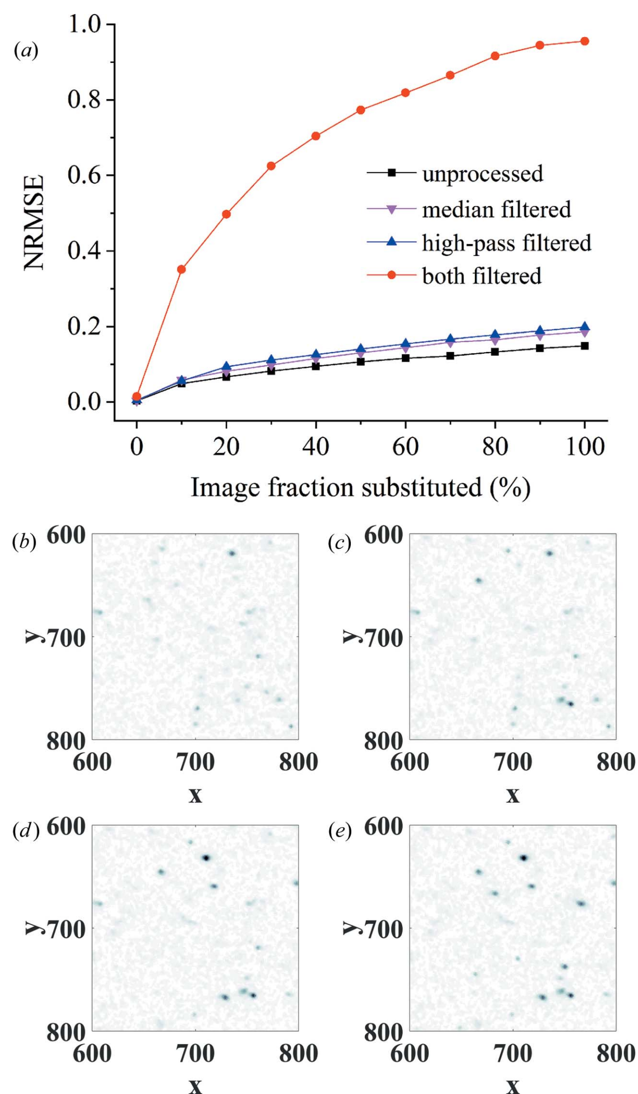

Figure 3
(*a*) Variation in registration error (NRMSE) between a reference pattern and a composite made by partly substituting a fraction of the reference pattern with another Laue pattern. Zero percent substitution represents two perfectly identical patterns, while 100% substitution represents two images with no overlap in diffraction spots. Among the filtering methods tested, sequential use of both the median filter and the high-pass filter is most successful in enhancing image differentiation by removing both detector noise and diffuse background signal. (*b*)–(*e*) show 0, 25, 50 and 100% substitution of the reference pattern (*b*) with the replacement pattern (*e*). For clarity only a sub-area of the full pattern is shown in each case.

and composite) to remove either detector damage noise (median filtering), background (high-pass filtering) or both.

Without any filtering a moderately low NRMSE value of 0.15 is obtained for the case of 100% image substitution, despite the fact that the diffraction spots in the two images arise from different sets of grains without any overlap. This is due to the non-changing background and the fixed position on the detector of any damaged pixels. One may thus erroneously infer a relatively good match between the two patterns. Median filtering and high-pass filtering applied individually improve the contrast (registration) difference by a small amount. However, the sequential use of both filters results in a significant enhancement of the differences between the two images, yielding an NRMSE value of 0.95. The large difference between using either one filter or both can be understood by the fact that both the damaged detector pixels and background signal have a strong influence on the image correlation calculation, so that only when both are removed is any significant improvement seen, with the image correlation returning information primarily related to the diffraction peak signals. Similar trends are seen as the overlap in image content is increased (towards 0% substitution), with the combined median and high-pass filter providing significantly improved differentiation of image pairs (*i.e.* larger NRMSE values). Lower values of the NRMSE (*i.e.* as obtained without filtering, or using only median or high-pass filtering individually) may reduce the robustness of the algorithm used for sample alignment and possibly lead to registration failure. Appropriate filtering of the diffraction patterns is, therefore, recommended for the application of the Laue-CC alignment technique.

3. Experimental demonstration

The proposed method for sample alignment was demonstrated using an *in situ* tensile experiment conducted at beamline 34-ID-E at the Advanced Photon Source, Argonne National Laboratory, where the experimental objective was to map the crystal lattice orientations in a volume of material both before and after a series of deformation steps using DAXM (Larson *et al.*, 2002). The sample for this experiment is pure Al (99.9%) prepared by spark plasma sintering, the detailed processing of which can be found elsewhere (Le *et al.*, 2013). The as-sintered sample has a nearly random texture and an average grain size of 2.5 µm, as measured by electron backscatter diffraction. Dog-bone tensile specimens were cut from the sintered discs by electron discharge machining, with gauge length, width and thickness of 12, 1.8 and 0.6 mm, respectively.

For the synchrotron measurements, a polychromatic X-ray beam with energies in the range of 7–30 keV was focused using two non-dispersive Kirkpatrick–Baez mirrors, producing a beam of near-Lorentzian profile with a full width at half-maximum of ~0.3 µm. The tensile specimen was mounted on a push-to-pull tensile device designed in-house that offers a nominal strain resolution of ~0.05% (C. L. Zhang *et al.*, 2017), and then installed at a 45° incident angle towards the X-ray beam, as required by the DAXM setup. The diffraction signal was recorded on a Perkin–Elmer flat-panel detector (409.6 × 409.6 mm, 2048 × 2048 pixels, amorphous Si, CsI scintillator, 16 bit dynamic range corresponding to 65 536 counts) mounted in 90° reflection geometry, 510.9 mm above the sample (see left-hand side of Fig. 1).

During the experiment the specimen was sequentially loaded to three strains of 0.15, 0.30 (near the conventionally defined yield point) and 0.80%. The first two deformation steps were carried out *in situ*. For the last deformation step (to a strain of 0.80%), the stage was first unmounted, then the sample was loaded and finally the stage was repositioned, providing an additional test of the applicability of the sample alignment method for *ex situ* experiments.

At the beginning of the experiment, and after each deformation step, DAXM was used to map a volume of dimensions 15.5 × 2.5 × 65 µm, using a step size of 0.5 µm along all axes. For the 3D mapping, a Pt wire of 100 µm in diameter was used as differential aperture, translated continuously in a plane parallel to the sample surface at a distance of ~250 µm. In this technique the X-ray microbeam is fixed and the sample stage is moved to illuminate different parts of the sample. Note that the accuracy of the sample stage positioning (and hence the beam position on the sample) is ~0.1 µm. A data collection time of ~8 h was required to obtain the crystal lattice orientations for all voxels in the investigated volume for each step of the experiment. The Laue-CC technique described in Section 2 was used, with the sample movement correction carried out after each deformation step.

3.1. Sample movement correction

The Laue-CC method was first tested by collecting patterns in a square grid before and after applying a small sample shift (without any sample deformation), and verifying that the correlation peak returned correctly the known sample shift. When this test proved successful, the Laue-CC approach was used, and further tested, during an *in situ* tensile experiment.

Fig. 4 shows the first step of the position alignment procedure for the 0.15% deformation step. Before deformation a Laue diffraction pattern was first collected with the microbeam in the centre of the region of interest on the sample surface [Fig. 4(*a*): note that here for better visibility we only show a sub-area of the pattern – the full pattern with 2048 × 2048 pixels was used in all calculations]. After straining to 0.15%, the sample stage was scanned to move the microbeam over the sample surface in a square 11 × 11 grid using a step size of 2 µm [see Fig. 4(*b*)], centred around the stage position after straining. A Laue diffraction pattern was collected at each point in this grid. The grid size was chosen to be sufficiently large to cover the maximum expected sample movement resulting from the applied strain, based on the known sample gauge length.

The patterns in the 11 × 11 grid were then each compared with the initial reference pattern (taken before deformation) according to the approach described in Section 2, and for each pattern the value of the NRMSE was determined. The results are plotted in Fig. 4(*b*), where it is seen that a well defined

minimum is obtained (indicated by a red box), with an NRMSE value of 0.25. The position of this minimum at (3, 2) with respect to the grid centre [shown by a cross in Fig. 4(*b*)] reveals sample shifts of 6 µm along the X axis and 4 µm along the Y axis during the applied deformation.

The diffraction pattern corresponding to this NRMSE minimum position is shown in Fig. 4(*c*). Additionally, as an example of the sensitivity of the Laue patterns to beam position, the Laue pattern at the (3, 0) grid position [the position marked by a blue box in Fig. 4(*b*)] is shown in Fig. 4(*d*). Good similarity is seen between the initial pattern [Fig. 4(*a*)] and the pattern corresponding to the NRMSE minimum [Fig. 4(*c*)]. The patterns in Figs. 4(*a*) and 4(*d*) show a large difference (NRMSE = 0.91), though some overlap of a few diffraction spots is still seen (indicated by red circles). This demonstrates that a misalignment of just 4 µm along the Y axis has a very significant effect on the NRMSE.

On the basis of the cross-correlation, the sample was moved so that the beam was at the position corresponding to the red box. The entire procedure (Laue pattern collection and image registration) takes only 5–10 min. For optimal alignment accuracy the entire procedure was repeated using a 1 µm step-size grid, and then repeated again using a 0.5 µm step-size grid before starting the next DAXM mapping. A similar alignment routine was performed after the second and third deformation steps (strains of 0.30 and 0.80%). In the case of the third deformation step, however, where the sample stage was removed and remounted, an initial estimate of the volume centre position was made using an optical microscope mounted on the DAXM setup (accuracy of ~10 µm), and the alignment procedure was terminated after the 1 µm grid scan.

To validate the accuracy in sample position alignment, the 3D microstructure of the characterized volume after each deformation step was reconstructed using the *LaueGo* (Tischler, 2014) software package at 34-ID-E, and these volumes were examined to determine the extent of overlap between them. Figs. 5(*a*) and 5(*b*) show the reconstructed volumes for the undeformed (initial) state and after straining to 0.15%, with voxels coloured according to their orientation. The similarity of the two images demonstrates qualitatively that the Laue-CC technique is successful. To quantify the accuracy, the shifts in position of the measured volume after each straining step compared with the initial volume position were determined by cross-correlation of the orientation data (Lin *et al.*, 2010). The results are summarized in Table 1

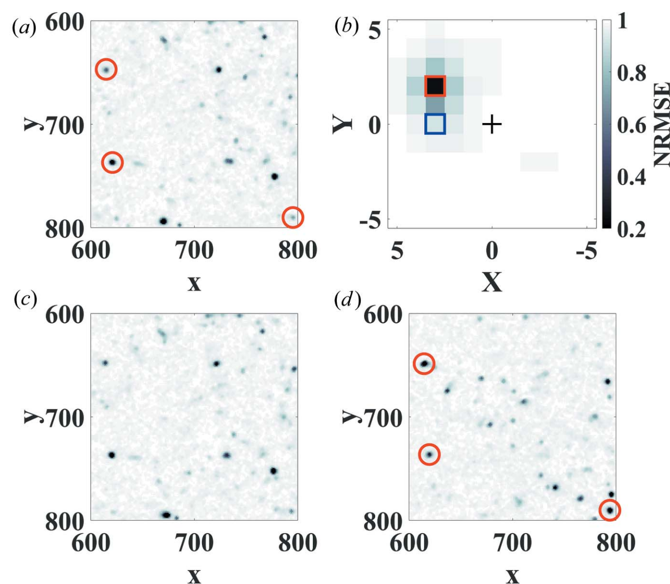

Figure 4
Illustration of the Laue-CC sample alignment procedure: (*a*) Reference pattern recorded from the centre position in the undeformed state. (*b*) Plot showing the variation of NRMSE between the reference and the patterns recorded after a strain of 0.15%, for an 11 × 11 grid of measured patterns, taken using a 2 µm step size and centred at the sample position after deformation. The red box shows the NRMSE minimum. (*c*) Laue diffraction pattern from the sample position corresponding to the red box (NRMSE minimum) in (*b*). Comparison with (*a*) confirms a high degree of similarity in the two patterns. (*d*) Laue diffraction pattern from the position marked by a blue box in (*b*), at a distance of about 4 µm to the prior centre. Some overlap in diffraction spots is present (examples are marked by circles), but many new spots are also seen. For visualization purposes only a sub-area of the full diffraction images is shown.

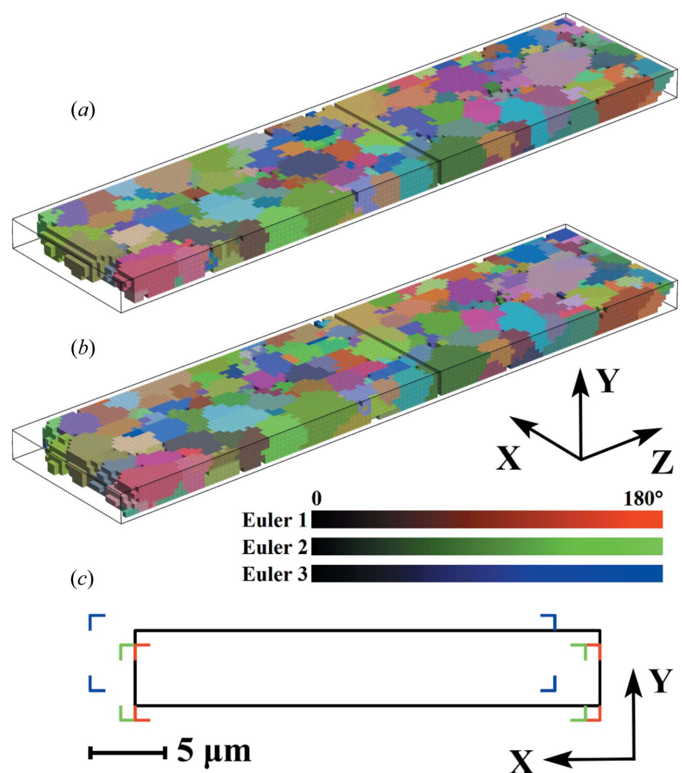

Figure 5
Illustration of the accuracy of the Laue-CC technique for sample alignment; reconstructed 3D grain maps of the characterized volumes at strains of (*a*) 0% (undeformed) and (*b*) 0.15%. The reconstructed volumes are 15.5 × 2.5 × 65 µm with a step size of 0.5 µm along all axes, with each voxel coloured according to the Euler angles in the description closest to $\{\varphi_1, \Phi, \varphi_2\} = \{90^\circ, 90^\circ, 90^\circ\}$ according to the colour key shown. (*c*) View along the Z axis (XY cross section) at a depth of 38 µm in each reconstructed volume [shown in (*a*) and (*b*) by black lines] illustrating the residual sample misalignment along the X and Y axes for the mapped volumes. The black rectangle shows the undeformed volume; the red, green and blue corner markers show the relative positions of the volumes mapped at strains of 0.15, 0.30 and 0.80%, respectively.

Table 1
Summary of the sample alignment data.

All values are relative to the undeformed sample position. 'Correction' gives the shift found using the Laue-CC method. 'Error' gives the accuracy of this correction based on inspection of overlap in the reconstructed mapped volumes.

	Movement		Rotation	
Strain (%)	Correction (μm)	Error (μm)	Angle (°)	Axis
0.15	[−6.0, −4.0]	[0, 0.5]	0.090 ± 0.003	[−0.41, 0.48, −0.78]
0.30	[−6.5, −7.7]	[−0.5, 0.5]	0.066 ± 0.006	[−0.52, 0.45, −0.72]
0.80	[4.5, −45.5]	[−1.5, 0.5]	0.097 ± 0.019	[0.20, −0.51, 0.84]

(column headed 'Error') and illustrated in Fig. 5(*c*), which shows a cross section through the volume at fixed depth along the *Z* axis and illustrates the residual misalignment after application of the Laue-CC technique. In general, a sample repositioning accuracy of 0.5 μm is achieved along both the *X* and *Y* axes. The residual error along the *X* axis after straining to 0.80% is slightly larger, though as noted above for this a final sub-micrometre step-size alignment scan was not carried out. Note that the assessment of the accuracy in sample alignment depends also on the step size used in the mapping and in the 3D reconstruction, as the voxel size is the smallest unit available for assessment.

The column in Table 1 headed 'Correction' lists the shifts needed to reposition the sample (*i.e.* the shift resulting from each deformation step). The larger correction required after the 0.80% deformation step (a *Y*-axis shift of over 40 μm) is accounted for by the removal and remounting of the loading stage for this deformation step. On the basis of the final mapped volume, at this strain a dis-registry after correction along the *X* axis of 1.5 μm was still found. This is due to the lack of a final 0.5 μm grid (see above) and the larger incremental strain step used (0.50%). It is expected that this could be ameliorated by applying the deformation in smaller steps and making incremental adjustments to the sample alignment. In all cases, by comparing the repositioning values with the map dimensions, it can be readily seen that without the use of sample repositioning the shifts along the *Y* axis are so large that the volumes before and after deformation would fail to overlap even partially, underlining the critical importance of the sample repositioning.

3.2. Sample rotation correction

Unlike sample position alignment, which is performed during the data collection process, sample rotation correction is performed only as a post-processing method, as fine rotation control of the sample stage is not available. As shown in the following, however, a correction for small rigid-body rotation after each straining step is valuable from the point of view of data analysis of the crystal lattice rotations developed in each grain during deformation.

To perform this correction, two Laue patterns are required, taken with the X-ray beam incident at the same surface location in a sample both before and after a given deformation step (in the following this is ensured by using the final adjusted sample volume positions, also taking account of the residual sample position errors listed in Table 1). For each pair of patterns, a total of 97 ROIs, each of size 512 × 512 pixels, were selected, evenly distributed by shifts of 128 pixels along the detector *x* and *y* axes (see Fig. 2). From these ROIs a series of vector shifts representing the displacement field over the Laue pattern were determined as described in Section 2.2. This was repeated for all incident beam positions where there was an overlap between the undeformed and deformed states [corresponding to the overlap in the rectangular cross sections shown in Fig. 5(*c*)], allowing an average displacement field to be calculated.

The result for the 0.15% strain step, based on the rotation relative to the undeformed state, is shown in Fig. 6. The sample rotation was then determined by a least-squares method, minimizing the sum of the squared error between the measured displacement field (vector shifts) and those calculated from the model function used to describe the sample orientation. A similar procedure was used to determine the rotation relative to the undeformed state for the sample after deformation to 0.30 and 0.80%. The results for all three deformation steps are summarized in Table 1. In each case the detected sample rotation angle is ~0.1°. The angular error (defined as the average angle between the diffraction vectors in the detected and final fitted displacement sets, and used here to define the precision in the rotation correction) increases, however, with strain, reflecting an increasing variation in the displacement field due to crystallographic lattice rotations accompanying plastic deformation, with a typical value of ~0.01°. The abrupt change of rotation axis for the 0.80% strain step is attributed to the *ex situ* experimental procedure, where a small inclination of the sample was presumably introduced during remounting of the sample.

Although these rigid-body sample rotation angles are small in absolute value, they are large relative to the expected pattern of lattice rotations due to the plastic deformation.

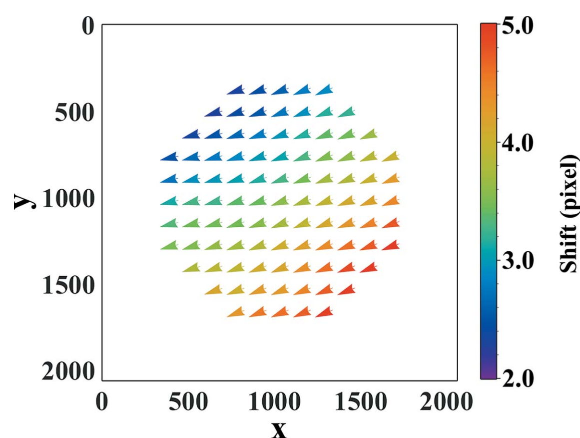

Figure 6
Plot showing the experimentally determined displacement field of the Laue diffraction spots for the sample after 0.15% strain, relative to the undeformed state. The arrows indicate the direction of the vector shift at each indicated position on the detector; the colouring indicates the magnitude.

Such lattice rotations provide essential information regarding the nature of grain subdivision during deformation, and the ability to obtain this information is one advantage of 3D nondestructive studies, where both the initial grain orientation and the final orientation at all voxels in a grain are known at each deformation step.

To demonstrate the importance of correcting for the sample rotation in revealing such information, 3D plots for individual grains were constructed, showing separately the misorientation angle and axis of each voxel in the deformed state relative to the orientation of the same voxel in the undeformed state (Hong *et al.*, 2017). An example for a grain in the sample deformed to 0.15% strain is given in Fig. 7, where plots are shown both with and without correction for the sample rotation. After correction the lattice rotations in this grain can be resolved in the rotation axis plot (in particular the presence of microstructural subdivision of the grain), whereas without the correction this plot is dominated by the sample rotation error, with the map showing only weak variation in the shade of green from voxel to voxel. A similar pattern of orientation variation in the deformed sample after application of the sample rotation correction is revealed by plots of the signed individual vector components of the misorientation between the initial orientation and each voxel expressed as a Rodrigues–Frank vector. For investigations where the applied deformation is small, for example studies of plastic yielding, it can be concluded that correction of the sample rotation during loading is required to reveal quantitatively the lattice rotations accompanying deformation.

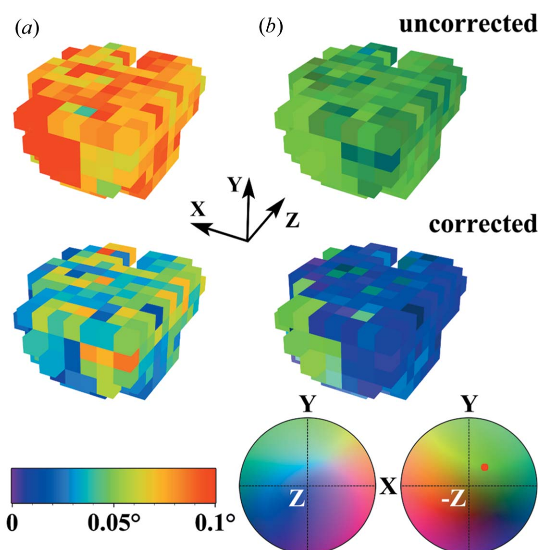

Figure 7
3D plots for a grain after deformation to a strain of 0.15%, showing for each voxel the rotation between the undeformed and deformed state, either uncorrected or corrected for rigid-body sample rotation (upper and lower sets of images, respectively): (*a*) the misorientation angle component and (*b*) the rotation axis component expressed in the beamline coordinate system. A scale bar for the misorientation angle and rotation axis colouring keys are given. The red dot in the right-most axis colouring key indicates the axis for the sample rotation correction at this strain. It can be seen that without correction the rotation axis plot is totally dominated by the sample rotation.

3.3. Comparison with other sample alignment approaches

The approach here to achieve sub-micrometre resolution in sample alignment has been developed for experiments where the goal is to map the same volume after a number of steps, where each step (mechanical loading, heating, charging *etc.*) may lead to some relative movement of the volume of interest with respect to the X-ray beam. The simplest alternative solution would be to map a sufficiently large volume each time to ensure sufficient overlap of the volumes. This, however, is very inefficient, and in the case of the example presented here impractical, as the data collection time for the 15.5 × 2.5 × 65 µm volume (31 × 5 × 130 voxels, with a step size of 0.5 µm) is already 8 h.

Other methods of alignment correction are possible. One already mentioned in the text is the use of Pt or Au markers deposited using a focused ion beam. These can be detected, for example, using a fluorescence signal or using micro-computed tomography (Shade *et al.*, 2016), but in each case this requires that a suitable additional detector is installed on the beamline and is considerably slower. Another approach that can be considered is the use of an optical camera to track surface features (either inherent or applied as markers). If the surface height changes (as is the case in tensile deformation), such an approach requires refocusing (hence additional sample movement) and only allows a spatial resolution of 5–10 µm, owing to the limited depth of field available using an optical camera. The proposed method, in contrast, uses the X-ray beam to track the sample position and is not therefore affected by sample height changes. This is because at any given beam position all material along the beam path is probed. So as long as the initial wire position is chosen conservatively, the sample surface position is found as a result of the DAXM measurements, with diffraction patterns available at all positions along the beam path from the surface of the sample to an interior depth limited only by signal attenuation and/or the chosen range of wire movement. Similarly any shift in the Z position due to a coupled translation with movement along the Y axis will not affect the indexing (for example, as the detector pixel size is 200 µm, a shift in Z axis of a few micrometres will only lead to a negligible change in the diffraction angles compared with our angular resolution). Also, as demonstrated in this study, the technique has a resolution that depends on the beam-movement step size, allowing sub-micrometre resolution in positioning accuracy.

Some limitations of the approach presented here nevertheless exist. The key limitation is that there should be sufficient variation in diffraction resulting from sample movement to allow a well defined peak to be found using DIC of Laue patterns. For coarser-grain structures, fewer grains will be illuminated, and thus some loss in sharpness in the cross-correlation peak may be expected, leading to larger repositioning errors. A final limitation is that in mechanical loading studies the method can only be used for small levels of plastic deformation, as once the diffraction spots become appreciably streaked the cross-correlation calculations become less reliable. For the experimental data we have analysed so far, the maximum in-grain variation where we have successfully used

the technique corresponds to a local orientation gradient of 0.25° μm^{-1}.

4. Summary

Reliable alignment of the sample position is critical for *in situ* synchrotron X-ray experiments. In this work, we have presented an alignment method based on cross-correlation of Laue microbeam diffraction images, requiring no pre-made surface features or markers. Demonstration of the method on a sample of Al with an average grain size of 2.5 μm, deformed by tension to a strain of 0.80%, shows that the method is sufficiently sensitive to small changes in diffraction patterns and allows determination of both sample movement and rotation. For the sample investigated here a repositioning accuracy of 0.5 μm is achievable, with a precision in sample rotation correction of ~0.01°. On the basis of its high efficiency and accuracy, this method is expected to be of widespread use for *in situ* studies requiring high-resolution 3D X-ray investigations.

Acknowledgements

Assistance from Ove Rasmussen on the design of the *in situ* loading device is gratefully acknowledged.

Funding information

The following funding is acknowledged: National Natural Science Foundation of China (grant No. 51671113; grant No. 51471095); US Department of Energy, Argonne National Laboratory (contract No. DE-AC02-06CH11357); Horizon 2020 (grant No. 788567).

References

Ahl, S. R., Simons, H., Zhang, Y. B., Detlefs, C., Stöhr, F., Jakobsen, A. C., Juul Jensen, D. & Poulsen, H. F. (2017). *Scr. Mater.* **139**, 87–91.

Balogh, L., Niezgoda, S. R., Kanjarla, A. K., Brown, D. W., Clausen, B., Liu, W. & Tomé, C. N. (2013). *Acta Mater.* **61**, 3612–3620.

Dingley, D. J., Wilkinson, A. J., Meaden, G. & Karamched, P. S. (2010). *J. Electron Microsc.* **59**, S155–S163.

Guizar-Sicairos, M., Thurman, S. T. & Fienup, J. R. (2008). *Opt. Lett.* **33**, 156–158.

Guo, Y., Collins, D. M., Tarleton, E., Hofmann, F., Tischler, J., Liu, W., Xu, R., Wilkinson, A. J. & Britton, T. B. (2015). *Acta Mater.* **96**, 229–236.

Hong, X., Godfrey, A., Zhang, C. L., Liu, W. & Chapuis, A. (2017). *Mater. Sci. Eng. A*, **693**, 14–21.

Johnson, G., King, A., Honnicke, M. G., Marrow, J. & Ludwig, W. (2008). *J. Appl. Cryst.* **41**, 310–318.

Larson, B. C. & Levine, L. E. (2013). *J. Appl. Cryst.* **46**, 153–164.

Larson, B. C., Yang, W., Ice, G. E., Budai, J. D. & Tischler, J. Z. (2002). *Nature*, **415**, 887–890.

Le, G. M., Godfrey, A. & Hansen, N. (2013). *Mater. Des.* **49**, 360–367.

Lin, F. X., Godfrey, A., Jensen, D. J. & Winther, G. (2010). *Mater. Charact.* **61**, 1203–1210.

Ludwig, W., Schmidt, S., Lauridsen, E. M. & Poulsen, H. F. (2008). *J. Appl. Cryst.* **41**, 302–309.

Margulies, L., Winther, G. & Poulsen, H. F. (2001). *Science*, **291**, 2392–2394.

Pantleon, W., Wejdemann, C., Jakobsen, B., Lienert, U. & Poulsen, H. F. (2009). *Mater. Sci. Eng. A*, **524**, 55–63.

Petit, J., Castelnau, O., Bornert, M., Zhang, F. G., Hofmann, F., Korsunsky, A. M., Faurie, D., Le Bourlot, C., Micha, J. S., Robach, O. & Ulrich, O. (2015). *J. Synchrotron Rad.* **22**, 980–994.

Poulsen, H. F. (2004). *Three-Dimensional X-ray Diffraction Microscopy: Mapping Polycrystals and Their Dynamics.* Berlin: Springer.

Poulsen, H. F. (2012). *J. Appl. Cryst.* **45**, 1084–1097.

Shade, P. A., Menasche, D. B., Bernier, J. V., Kenesei, P., Park, J.-S., Suter, R. M., Schuren, J. C. & Turner, T. J. (2016). *J. Appl. Cryst.* **49**, 700–704.

Simons, H., King, A., Ludwig, W., Detlefs, C., Pantleon, W., Schmidt, S., Stöhr, F., Snigireva, I., Snigirev, A. & Poulsen, H. F. (2015). *Nat. Commun.* **6**, 6098.

Sutton, M. A., Orteu, J. J. & Schreier, H. W. (2009). *Image Correlation for Shape, Motion and Deformation Measurements: Basic Concepts, Theory and Applications*. New York: Springer.

Tischler, J. Z. (2014). *Strain and Dislocation Gradients from Diffraction*, edited by R. Barabash & G. Ice, pp. 358–375. London: Imperial College Press.

Zhang, C. L., Zhang, Y. B., Wu, G. L., Liu, W., Juul Jensen, D. & Godfrey, A. (2017). *IOP Conf. Ser. Mater. Sci. Eng.* **219**, 012050.

Zhang, F. G., Bornert, M., Petit, J. & Castelnau, O. (2017). *J. Synchrotron Rad.* **24**, 802–817.

Zhang, M., Pan, Y., Dorfman, R. G., Yin, Y., Zhou, Q., Huang, S., Liu, J. & Zhao, S. (2017). *Sci. Rep.* **7**, 7.